NJC

RSC Publishing

PAPER

View Article Online
View Journal | View Issue

Cite this: *New J. Chem.*, 2013, **37**, 3024

One-pot synthesis of water-stable gadolinium-doped $Yb(OH)CO_3$ nanoprobes for *in vivo* dual MR and CT imaging†

Yinhua Jin,[ab] Jianhua Liu,[cd] Quan Zheng,[b] Jun Xu,[b] Bhoj Raj Sharma,[c] Guilin He,[b] Min Yan,[b] Lin Zhang,[b] Yang Song,[b] Tao Li,[b] Qinghai Yuan,*[c] Yong Sun*[d] and Haishan Yang*[a]

Received (in Victoria, Australia) 19th May 2013,
Accepted 27th June 2013

DOI: 10.1039/c3nj00536d

www.rsc.org/njc

Molecular imaging techniques have shown increasing potential in the definition and imaging of the structure and function of biological systems for preclinical applications. Herein, we report a high-quality dual-modal imaging platform based on water-stable gadolinium-doped $Yb(OH)CO_3$ nanoparticles. These nanoprobes were prepared *via* a one-pot method, meeting the criteria for a biomedical material. Compared with iobitridol, which is routinely used in clinical applications, our $Yb(OH)CO_3$:Gd nanoparticles provided greatly enhanced contrast at regularly used clinical voltages. By virtue of their doping with gadolinium, these well-designed nanostructures could also be applied as an excellent MRI nanoprobe, which provided similar biodistribution results with our CT experiments. Detailed *in vitro* and *in vivo* toxicological study indicated that the uniformly sized nanoparticles possessed high biocompatibility and also low toxicity, making them safe for clinical use. The concept presented here shows great potential for the design and synthesis of nanoprobes with high imaging efficiency and low systemic toxicity.

Introduction

Along with the rapid development of modern engineering and technology, multifunctional nanomaterials have been frequently studied in the contexts of physics, chemistry, biology, as well as medicine owing to their excellent electric, magnetic, and optical properties.[1–5] Among these applications, nanodevices used as biomedicine contrast agents in various diagnostic imaging techniques including X-ray computed tomography (CT), single-photon emission computed tomography (SPECT), positron emission tomography (PET), magnetic resonance imaging (MRI), and ultrasonography (US) have attracted considerable attention.[6–14] However, each imaging modality has its own advantages and limitations, which can not satisfy the high requirements of efficiency and accuracy for the diagnosis and prognosis of diseases in the clinic.[15–20] For instance, CT is advantageous with regard to its deep tissue penetration, cost effectiveness, and high resolution, but its low sensitivity usually results in poor soft-tissue contrast. MRI has been widely applied in clinical diagnosis due to its high sensitivity and admirable soft-tissue contrast. However, MRI is unsuitable for imaging in patients who possess magnetic hardware, such as heart pacemakers or artificial hipbone joints. Considering that more complementary and effective information can be achieved from each imaging modality, multi-modal imaging is thus highly desirable for scientific research and clinical diagnosis.

Resulting from the distinctive physical and chemical properties of lanthanides, great effort has been devoted to the design and construction of lanthanide-based nanoparticulate contrast agents for molecular imaging. Among them, nanoparticles co-doped with Yb^{3+} and Er^{3+}/Tm^{3+} exhibit unique upconversion luminescence (UCL), which gives rise to a high signal-to-noise ratio (SNR) and deep light penetration for imaging *in vivo*.[21–24] Gd^{3+} ions with unpaired 4f electrons are paramagnetic and generally doped into different systems as nanoprobes for T_1-weighted or T_2-weighted MR imaging.[25–29] Gd-, Yb-, and Lu-based nanomaterials have been applied as CT contrast agents due to their higher imaging efficiency and longer blood circulation time than those of routinely used small iodinated molecules.[30–34] In particular, thanks to the

[a] *Department of Radiology, China-Japan Union Hospital of Jilin University, Changchun 130033, P. R. China. E-mail: dryanghs@gmail.com*
[b] *Department of Medical Imaging, The General Hospital of Jilin Chemical Group Corporation, Jilin 132022, P. R. China*
[c] *Department of Radiology, The Second Hospital of Jilin University, Changchun, 130041, P. R. China. E-mail: qinghaiyuan@gmail.com*
[d] *Department of Radiology, The Second Hospital of Kunming Medical University, Kunming, 650101, P. R. China. E-mail: dryongsun@yahoo.com*

† Electronic supplementary information (ESI) available: Supporting figures. See DOI: 10.1039/c3nj00536d

suitable K-edge energy and high earth abundance of ytterbium, Yb-based nanoparticles show greater potential for clinical use as a new generation of nanoparticulate CT contrast agents. Despite this great advancement, there still exist many intractable problems that hinder the development of this field, such as complicated synthesis routes and time-consuming techniques to prepare these contrast agents. More importantly, the ability to produce inexpensive and nontoxic nanoparticulate contrast agents *via* a facile large-scale route is urgently needed due to the large dose required in a daily imaging course.

The synthesis of colloidal single-lanthanide hydroxycarbonates and oxides has been achieved through a urea-based homogeneous precipitation (UBHP) method as long ago as 1986.[35] Inspired by a previous report, herein, we report a facile strategy to synthesize water-stable gadolinium-doped $Yb(OH)CO_3$ nanoparticles (denoted $Yb(OH)CO_3$:Gd) as a high-performance dual-modal contrast agent for use in X-ray CT and MR imaging. With their non-cytotoxic character and extremely low hemolysis, these nanoparticles show excellent imaging efficiency. In addition, detailed biodistribution, systematical toxicity, and possible clearance route are studied using a single-dose intravenous injection in a mouse model, indicating the overall safety of our dual-modal nanoparticulate contrast agent.

Materials and methods

Materials

Ytterbium nitrate pentahydrate ($Yb(NO_3)_3{\cdot}5H_2O$), gadolinium nitrate hexahydrate ($Gd(NO_3)_3{\cdot}6H_2O$), chloral hydrate, and urea were obtained from Aladdin Reagent. Dulbecco's modified Eagle's medium (DMEM), fetal bovine serum (FBS) and trypsin, were from Sangon. Iobitridol was purchased from Guerbet. Other reagents and solvents were acquired from Beijing Chemicals.

Preparation of $Yb(OH)CO_3$:Gd nanoparticles

The $Yb(OH)CO_3$:Gd nanoparticles were fabricated *via* a one-pot urea-based homogeneous precipitation process. Typically, $Yb(NO_3)_3{\cdot}5H_2O$ (6.0 mmol), $Gd(NO_3)_3{\cdot}6H_2O$ (1.5 mmol), and urea (250 mmol) were dissolved in deionized water. The total volume of the solution was about 500 mL. The above solution was first homogenized by magnetic stirring at room temperature for 2 h. Then, the resultant homogeneous solution was reacted at 90 °C for another 3 h in an oil bath. Through centrifugation a suspension was obtained, which was collected after washing with deionized water and ethanol in sequence. Finally it was dried under vacuum at 60 °C overnight for further use.

Measurements and characterization

The composition and morphology of the as-prepared samples were analyzed by a field emission scanning electron microscope (FESEM, S4800, Hitachi) equipped with an energy-dispersive X-ray spectrum. Transmission electron microscope (TEM) measurements were obtained on a JEOL JEM-2010EX TEM. X-ray powder diffraction (XRD) of the samples was performed on a D8 Focus diffractometer by using CuKα radiation (λ = 0.15405 nm). The concentrations were determined by inductively coupled plasma-mass spectrometry (ICP-MS). X-ray photoelectron (XPS) measurements were performed on an ESCALAB-MKII spectrometer (VG Co., United Kingdom). CT images were acquired using a 256-slice multidetector CT scanner (Brilliance iCT, Philips Healthcare, Cleaveland, Ohio, USA). T_1-weighted MRI images were acquired using a Siemens Espree 1.5 T unit.

Cell cultures

Cells were cultured in Dulbecco's modified Eagle's medium (DMEM) containing streptomycin (100 U mL^{-1}), 10% fetal bovine serum (FBS) and penicillin (100 U mL^{-1}), in a humidified incubator at 37 °C and 5% CO_2. The cells were cultured with the use of trypsin and were again put back into fresh complete medium before plating.

In vitro cytotoxicity studies

To quantify the cytotoxicity of $Yb(OH)CO_3$:Gd nanoparticles, MTT reduction assays were carried out. At first, the HepG2 cells were cultured in 96-well plates at a density of 5×10^3 per well for 12 h to allow the cells to attach. Afterwards, serial dilutions of different contrast agent formulations were added to the culture medium. At the end of the incubation time, the media containing nanoparticles were removed, and cell samples were treated with MTT for another 4 h, followed by the addition of dimethyl sulfoxide (DMSO) to dissolve the formazan crystals. For each treatment group, six replicates were done and the percentage viability was normalized to cell viability in the absence of contrast agent.

Cellular modality and observation

In a typical experiment, HepG2 cells with a density of 2×10^4 were plated in a 12-well plate for 4 h to allow the cells to attach. After washing the cells twice with cool phosphate-buffered saline (PBS), $Yb(OH)CO_3$:Gd nanoparticles (1 mg NPs mL^{-1}) were added to the cell culture medium. After 48 h of incubation, the cells were washed again several times with PBS to remove the remaining nanoparticles, and then observed using an optical microscope under white light.

In vitro hemolysis assay

The hemolysis assay experiments were carried out as an important factor to evaluate the *in vitro* biocompatibility. Firstly, a 1 mL blood sample was added to 2 mL of PBS, and the red blood cells (RBCs) were isolated from the serum by centrifugation at 8000 rpm for 10 min. After being washed five times with 5 mL of PBS solution, the purified blood was diluted to 1/10 of its volume with PBS solution. 0.2 mL of diluted RBC suspension was then mixed with (a) 0.8 mL of PBS as a negative control, (b) 0.8 mL of deionized water as a positive control, and (c) 0.8 mL of $Yb(OH)CO_3$:Gd nanoparticle suspensions with concentrations ranging from 0 to 1 mg NPs mL^{-1}. Then all of the mixtures were vortexed and kept at room temperature for 3 h. Finally, the mixtures were centrifuged at 12 000 rpm for 5 min, and the absorbance of supernatants at 541 nm was determined by UV-vis spectroscopy. The percent hemolysis of RBCs was calculated as follows: percent hemolysis = [(sample absorbance − negative control

absorbance)/(positive control absorbance − negative control absorbance)] × 100.

Animal administration

Wister rats and Kunming mice weighing about 400 g and 25 g respectively were bought from Laboratory Animal Center of Jilin University (Changchun, China). The procedures for their handling and care were under the jurisdiction and guidelines of the Regional Ethics Committee for Animal Experiments.

MR imaging

In vitro T_1-weighted MR images were acquired by using a 1.5-T clinical MRI instrument (Siemens Medical System). Dilutions of Yb(OH)CO_3:Gd nanoparticles in PBS buffer containing 1% agarose with expected different concentrations for use as a contrast agent were placed in a series of 4.0 mL Eppendorf tubes for T_1-weighted MR imaging. After careful preparation, the Eppendorf tubes were then scanned in a 1.5-T Magnetom Espree MIR system. *In vivo* experiments were performed on an anaesthetized Wister rat. The solution of Yb(OH)CO_3:Gd nanoparticles (10 mg mL^{-1}, 500 μL) was injected intravenously into the rat and images were collected at different timed intervals.

CT imaging

To assess CT contrast efficacy, Yb(OH)CO_3:Gd nanoparticles and iobitridol were dispersed in PBS buffer containing 1% agarose with different RE and I concentrations over the range of 0 to 25 mg mL^{-1}. After careful preparation, the Eppendorf tubes were scanned in a Philips CT imaging system.

For *in vivo* CT imaging, rats were first anaesthetized by injecting 10 wt% chloral hydrate intraperitoneally. Two rats were injected intravenously with 0.3 mL of iobitridol (clinical reagent and 350 mg I mL^{-1}) and 1.0 mL of Yb(OH)CO_3:Gd nanoparticle solution (50 mg RE mL^{-1}), respectively. CT images were acquired using a Philips 256-slice CT Scanner (Philips Medical System).

Biodistribution of Yb(OH)CO_3:Gd nanoparticles

Mice injected with Yb(OH)CO_3:Gd nanoparticles (20 mg NPs kg^{-1}) were sacrificed and their major organs were collected for quantitative analysis of Yb ions. The organs collected were removed surgically from the animal and then placed into a centrifuge tube containing 4 mL of aqua regia. After centrifugation, the tubes were kept in an incubator for 2 h under heat treatment (80 °C) for dissolution of the tissues. Finally, the obtained liquid was submitted for ICP-MS analysis.

In vivo body weight measurements

For these measurements, two groups of Kunming mice were separated into cages (n = 5). The test group was injected with Yb(OH)CO_3:Gd suspensions (in 0.9 wt% NaCl) at a total dose of 200 mg NPs kg^{-1} *via* the tail vein. The other group of Kunming mice received an injection of 0.9 wt% NaCl and were used as the control group. The body weight of the mice in both groups was recorded for 30 days.

Histology analysis

The mice from both the test and the control group, *i.e.* with or without Yb(OH)CO_3:Gd nanoparticles (200 mg NPs kg^{-1}), were sacrificed after 30 days. The collected tissues from the two groups were fixed in 10% neutral buffered formalin. Then, the collected tissues were embedded in paraffin, sectioned (4 μm thick), and stained with hematoxylin and eosin (H&E). The histological sections were observed under an optical microscope.

Results and discussion

A typical synthesis of uniform Yb(OH)CO_3:Gd nanoparticles was carried out *via* a facile urea-based homogeneous precipitation method (UBHP).[35] This classical method has been recognized as a general route for the preparation of lanthanide hydroxylcarbonate in which urea serves as a precipitation agent for metal ions due to its self-decomposition into OH^- and CO_3^{2-} at elevated temperature. As revealed by scanning electron microscopy (SEM) and transmission electron microscopy (TEM), these nanoparticles with a spherical and non-aggregated nature have a relatively smooth surface and a mean diameter of 120 nm (Fig. 1a and b). Wide-angle XRD and energy-dispersive spectroscopy (EDS) analysis showed that the nanostructures were amorphous and that the elements Yb, C, O, and Gd were present (Fig. 1c and d). As determined by ICP-MS, the actual molar ratio of Yb–Gd was close to 4 : 1. Compared with previous reports, our method possessed both the advantages of requiring no organic reagents and also providing a facile fabrication route.[36–38]

As shown in Fig. 2a, the results of FT-IR spectroscopy exhibited the characteristic adsorption bands of ν_{as}O–C–O (1530 and 1406 cm^{-1}), π-CO_3^{2-} (844 cm^{-1}), and δ-CO_3^{2-} (762 and 696 cm^{-1}), demonstrating the presence of a carbonate group. As can be seen in the inset photos of Fig. 2a, our

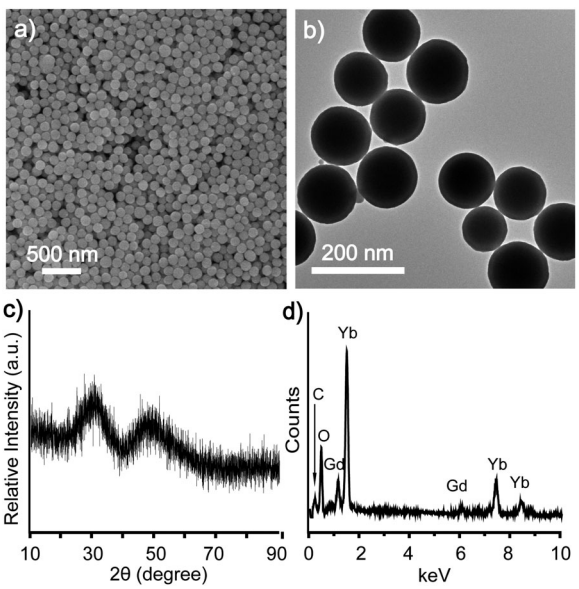

Fig. 1 SEM image (a), TEM micrograph (b), wide-angle XRD pattern (c) and EDS spectrum (d) of Yb(OH)CO_3:Gd nanoparticles.

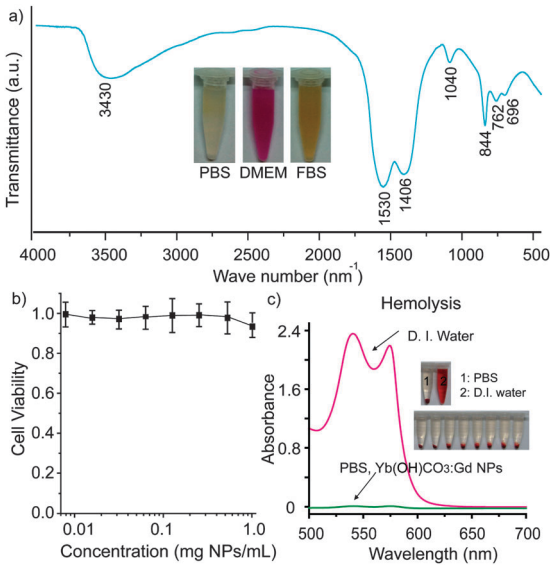

Fig. 2 The FT-IR spectrum of $Yb(OH)CO_3$:Gd nanoparticles (a). Inset: photos of $Yb(OH)CO_3$:Gd nanoparticles in various solutions including phosphate buffered saline (PBS), fetal bovine serum (FBS), and DMEM cell medium. Effect of $Yb(OH)CO_3$:Gd nanoparticles on the viability of HepG2 cells (b). Concentration-dependent hemolysis of $Yb(OH)CO_3$:Gd nanoparticles (c). Inset: photographic images for direct observation of hemolysis by the visible formation of nanostructures.

nanoparticulate contrast agent exhibited excellent stability without any noticeable aggregation in various physiological solutions. From the viewpoint of clinical diagnosis and prognosis, contrast agents must be non-toxic both *in vitro* and *in vivo*. *In vitro* cytotoxicity was evaluated by the MTT assay, which was exposed to incubation of $Yb(OH)CO_3$:Gd nanoparticles for 48 h, and the subsequent results of the viability of the HepG2 cells showed that more than 90% cells survived (Fig. 2b). In the presence of our nanoparticles at a concentration of 1 mg NPs mL^{-1}, microscopy images of HepG2 cells shown in Fig. S1 (ESI†) revealed that all cells spread and proliferated equally. *In vitro* hemolytic assay was further applied to evaluate the blood compatibility. Photographic images in Fig. 2c and detailed data in Table S1 (ESI†) revealed that nearly no hemolysis of RBCs could be detected at the experimental concentration of 1 mg NPs mL^{-1}, indicating the excellent blood compatibility of our nanoparticles and their feasibility for use in *in vivo* dual-modal imaging.

Gadolinium-based agents have been used clinically as efficient MR contrast agents, therefore the feasibility of our nanoparticulate contrast agent as a powerful MR contrast agent is expected. Fig. 3a shows the $1/T_1$ dependence of the Gd^{3+} concentration. The r_1 value of the $Yb(OH)CO_3$:Gd nanoparticles was 12.7 mM^{-1} s^{-1} which is higher than the value of the pure Gd–DTPA complex (r_1 = 4.08 mM^{-1} s^{-1}), indicating that the enhancement of the MR signal by our nanoparticulate contrast agent was higher than that of the routinely used clinical agent. As shown in Fig. 3b, a positive enhancement in MR signal was observed for all tubes compared with water. Furthermore, the T_1-weighted MR images brightened with an increase in the concentration, indicating that the $Yb(OH)CO_3$:Gd nanoparticles could be used as an effective MRI contrast agent. The application of MR imaging *in vivo* for small animals was further evaluated by intravenous injection of our well-defined contrast agents into rats. The positive-contrast enhancement of the nanoprobes was studied anatomically by transversal MR imaging *in vivo*. As shown in Fig. 3c, the detectable T_1-weighted contrast enhancements were observed in the liver area, as further evidenced by the changes of signal intensities. The positive-contrast increased gradually with time (Fig. S2, ESI†). For the kidney, nearly no enhancement occurred due to the more effective accumulation of nanoparticles by macrophages in the liver during blood circulation. From the above evaluation, these results indicated that our $Yb(OH)CO_3$:Gd nanoparticles could be potentially applied as a MRI positive-contrast agent *in vivo*.

To evaluate CT contrast efficacy, we compared the X-ray absorption of $Yb(OH)CO_3$:Gd nanoparticles to that of iobitridol. With an increase in contrast agent concentration, both agents

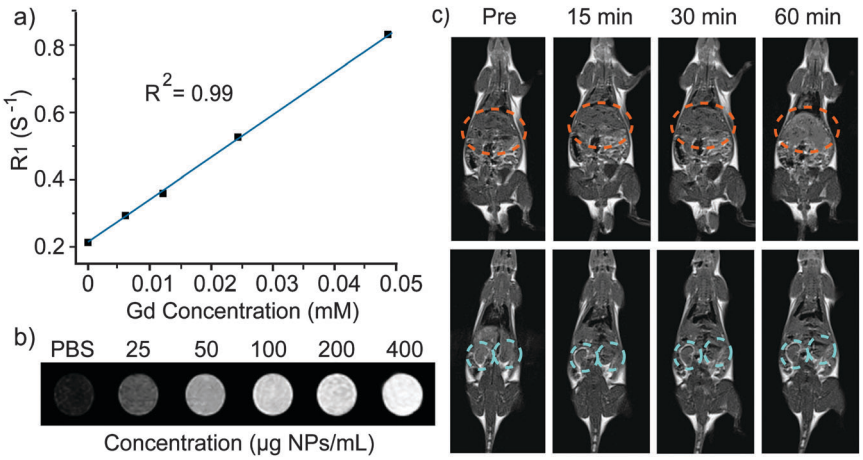

Fig. 3 Plot of R_1 ($1/T_1$) as a function of Gd concentrations in water (a). T_1-weighted MR images of $Yb(OH)CO_3$:Gd nanoparticles based on different nanoparticle concentrations (b). *In vivo* T_1-weighted MR images of a rat before and after intravenous injection of $Yb(OH)CO_3$:Gd nanoparticles at different time intervals (c). Injected dose: 0.5 mL of $Yb(OH)CO_3$:Gd nanoparticles solution (10 mg NPs mL^{-1}).

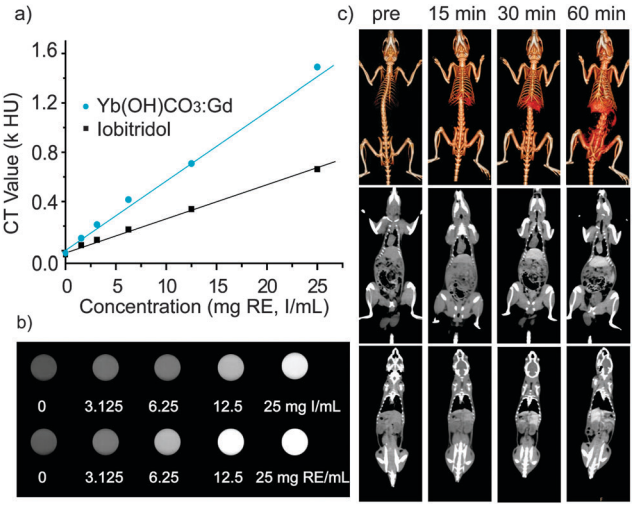

Fig. 4 CT values and *in vitro* CT images of $Yb(OH)CO_3$:Gd nanoparticles and iobitridol as a function of RE and I concentrations (a and b). *In vivo* serial CT view images of rats after intravenous injection of $Yb(OH)CO_3$:Gd nanoparticles. Injected doses: 0.3 mL of iobitridol (350 mg I mL^{-1}) and 1.0 mL of $Yb(OH)CO_3$:Gd nanoparticles solution (50 mg RE mL^{-1}).

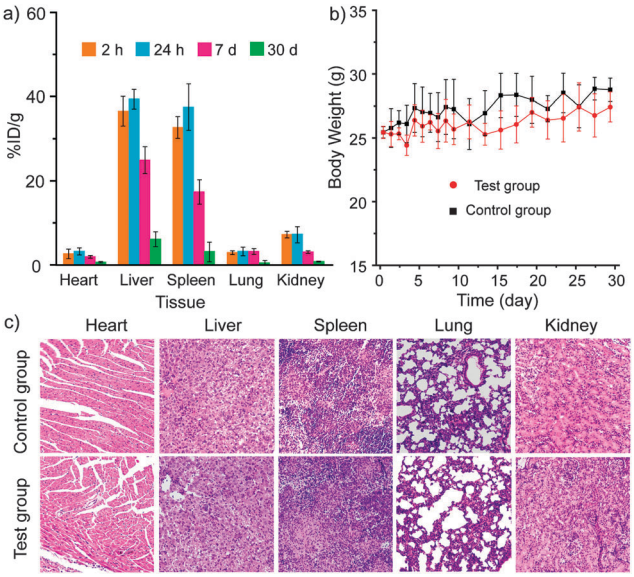

Fig. 5 Time-dependent biodistribution of $Yb(OH)CO_3$:Gd nanoparticles in mice (a). Change in body weight measured from mice injected with and without $Yb(OH)CO_3$:Gd nanoparticles (b). Histological changes of mice after intravenous injection of a single dose of contrast agent solution and 0.9% NaCl solution (c).

exhibited signal enhancement. A good linear correlation between the Hounsfield units (HU) value and the concentration of RE or I was observed. The results shown in Fig. 4a revealed that the X-ray absorption of $Yb(OH)CO_3$:Gd nanoparticles was much higher than that of iobitridol at equivalent concentrations. Otherwise, contrast images obtained from the above concentrations revealed the same results (Fig. 4b). Therefore, our contrast agent exhibited greatly superior performance to that of clinically used small iodinated molecules. Encouraged by the high CT contrast performance in this primary experiment, we further evaluated our contrast agent's application in CT imaging by intravenous injection of our nanoparticles, and assessment of the biodistribution of contrast agent tracked by X-ray CT imaging at different time intervals. As illustrated in Fig. 4c, after injection of the solution containing $Yb(OH)CO_3$:Gd nanoparticles, a clear enhancement of the signals from the liver was observed at an early time (15 min). Remarkably, the gradual enhancement of signals from the liver and spleen continued for over 1 h. Upon closer inspection of the 3D-renderings of CT images, they additionally display evident enhancement in the liver-vessel signals within the same period of time. Detailed HU values of these organs at timed intervals are shown in Table S2 (ESI†). Another rat was selected as a negative control by intravenous injection of iobitridol. As shown in Fig. S3 (ESI†), no obvious enrichment in heart, liver, lung, or spleen signals could be detected after intravenous administration of iobitridol. Nearly all of the contrast agent accumulated in the urinary organs, such as kidneys and bladder, within a short period of time (Table S3, ESI†). The short time in circulation, in addition to the rapid vascular permeation of clinical small iodinated molecules, limited the use of iobitridol for targeted imaging and angiography.

To obtain more accurate biodistribution of $Yb(OH)CO_3$:Gd nanoparticles in small animals, we collected mouse organs at different time points after intravenous administration. As shown in Fig. 5a, our contrast agents mainly accumulated in the reticuloendothelial system (RES) such as the liver and spleen, similar to our CT imaging results shown in Fig. 4c. To provide conclusive evidence for the metabolic route, Yb content measurements in mouse excretions were further performed. Our results indicated that the clearance of our nanoparticles was possibly through both renal and fecal excretions (data not shown). Considering the long retention time of $Yb(OH)CO_3$:Gd nanoparticles *in vivo*, the long-term toxicology was studied. The body weights of the test group increased slightly in a pattern similar to those of the control group (Fig. 5b). Histological assessment was performed to further determine whether these nanoparticles caused any tissue damage or exerted any other toxic effect on organs. Our results indicated that nearly no noticeable tissue damage or any other toxic effect on organs occurred (Fig. 5c and Fig. S4, ESI†). For hematology and blood biochemical assay, there was nearly no difference between the control group and treatment group 30 d after injection (Table S4, ESI†), indicating that our well-prepared nanoparticulate contrast agents revealed high *in vivo* compatibility.[39–42]

Conclusions

In conclusion, we have reported a facile strategy to construct a monodisperse dual-modal nanoparticulate contrast agent based on $Yb(OH)CO_3$:Gd nanoparticles through a classical urea-based homogeneous precipitation method. In addition to the detailed characterization of the $Yb(OH)CO_3$:Gd nanoparticles, evaluation of both cytotoxicity and hemolysis demonstrated their excellent biocompatibility, indicating their possible application for use in MR and CT imaging *in vivo*. Compared with routinely used

iobitridol, our nanoparticles could provide much more obvious enhancement at clinical voltages of 120 kVp. By doping with gadolinium, our nanoparticulate contrast agent could simultaneously perform perfect MR imaging, revealing similar organ signal enrichment and bio-distribution with our CT imaging results. In addition, detailed *in vivo* toxicological study including histological assay, body weight measurement, hematology, as well as blood biochemical assay, further indicated that our dual-modal nanoparticulate contrast agent exhibited overall safety. Last but not least, our lanthanide–hydroxycarbonate nanoprobes exhibited more advantages over previously reported lanthanide-doped fluoride, such as easy decomposition inside macrophage cells after RES uptake and near total excretion from bodies within a month.

Acknowledgements

Financial support was provided by the technology development project of National Development and Reform Commission of Jilin province (No. JF2012c007-1).

References

1 J. Barreto, W. O'Malley, M. Kubeil, B. Graham, H. Stephan and L. Spiccia, *Adv. Mater.*, 2011, **23**, H18.
2 J. Kim, Y. Piao and T. Hyeon, *Chem. Soc. Rev.*, 2009, **38**, 372.
3 H. Yang and Y. Xia, *Adv. Mater.*, 2007, **19**, 3085.
4 G. Maltzahn, J. Park, A. Agrawal, N. Bandaru, S. Das, M. Sailor and S. Bhatia, *Cancer Res.*, 2009, **69**, 3892.
5 W. Cai and X. Chen, *Small*, 2007, **3**, 1840.
6 J. Yang, C. Favazza, R. Chen, J. Yao, X. Cai, K. Maslov, Q. Zhou, K. Shung and L. Wang, *Nat. Med.*, 2012, **18**, 1297.
7 M. Kircher, A. Zerda, J. Jokerst, C. Zavaleta, P. Kempen, E. Mittra, K. Pitter, R. Huang, C. Campos, F. Habte, R. Sinclair, C. Brennan, I. Mellinghoff, E. Holland and S. Gambhir, *Nat. Med.*, 2012, **18**, 829.
8 R. Kumar, M. Nyk, T. Ohulchanskyy, C. Flask and P. Prasad, *Adv. Funct. Mater.*, 2009, **19**, 853.
9 S. Zeng, M. Tsang, C. Chan, K. Wong and J. Hao, *Biomaterials*, 2012, **33**, 9232.
10 J. Zhou, M. Yu, Y. Sun, X. Zhang, X. Zhu, Z. Wu, D. Wu and F. Li, *Biomaterials*, 2011, **3**, 1148.
11 K. Park, S. Lee, E. Kang, K. Kim, K. Choi and I. Kwon, *Adv. Funct. Mater.*, 2009, **19**, 1553.
12 S. Chou, Y. Shau, P. Wu, Y. Yang, D. Shieh and C. Chen, *J. Am. Chem. Soc.*, 2010, **132**, 13270.
13 T. Skotland, *Contrast Media Mol. Imaging*, 2012, **7**, 1.
14 C. Alric, J. Taleb, G. Duc, C. Mandon, C. Billotey, A. Meur-Herland, T. Brochard, F. Vocanson, M. Janier, P. Perriat, S. Roux and O. Tillement, *J. Am. Chem. Soc.*, 2008, **130**, 5908.
15 W. Seo, J. Lee, X. Sun, Y. Suzuki, D. Mann, Z. Liu, M. Terashima, P. Yang, M. Mcconnell, D. Nishimura and H. Dai, *Nat. Mater.*, 2006, **5**, 971.
16 J. Cheon and J. Lee, *Acc. Chem. Res.*, 2008, **41**, 1630.
17 J. Jung, M. Kim, J. Cho, S. Lee, I. Yang, J. Cho, S. Kim, C. Lee and J. Park, *Biomaterials*, 2012, **33**, 5865.
18 H. Wang, L. Zheng, C. Peng, R. Guo, M. Shen, X. Shi and G. Zhang, *Biomaterials*, 2011, **32**, 2979.
19 X. Ma, H. Tao, K. Yang, L. Feng, L. Cheng, X. Shi, Y. Li, L. Guo and Z. Liu, *Nano Res.*, 2012, **5**, 199.
20 W. Rieter, J. Kim, K. Taylor, H. An, W. Lin, T. Tarrant and W. Lin, *Angew. Chem., Int. Ed.*, 2007, **46**, 3680.
21 H. Xing, W. Bu, Q. Ren, X. Zheng, M. Li, S. Zhang, H. Qu, Z. Wang, Y. Hua, K. Zhao, L. Zhou, W. Peng and J. Shi, *Biomaterials*, 2012, **33**, 5384.
22 G. Tian, Z. Gu, L. Zhou, W. Yin, X. Liu, L. Yan, S. Jin, W. Ren, G. Xing, S. Li and Y. Zhao, *Adv. Mater.*, 2012, **24**, 1226.
23 L. Cheng, K. Yang, S. Zhang, M. Shao, S. Lee and Z. Liu, *Nano Res.*, 2010, **3**, 722.
24 A. Xia, Y. Gao, J. Zhou, C. Li, T. Yang, D. Wu, L. Wu and F. Li, *Biomaterials*, 2011, **32**, 7200.
25 I. Li, C. Su, H. Sheu, H. Chiu, Y. Lo, W. Lin, J. Chen and C. Yeh, *Adv. Funct. Mater.*, 2008, **18**, 766.
26 Z. Liu, X. Liu, Q. Yuan, K. Dong, L. Jiang, Z. Li, J. Ren and X. Qu, *J. Mater. Chem.*, 2012, **22**, 14982.
27 M. Deng, Y. Ma, S. Huang, G. Hu and L. Wang, *Nano Res.*, 2011, **4**, 685.
28 F. Chen, P. Huang, J. Zhu, J. Wu, C. Zhang and D. Cui, *Biomaterials*, 2011, **32**, 9031.
29 P. Sharma, N. Bengtsson, G. Walter, H. Sohn, G. Zhou, N. Iwakuma, H. Zeng, S. Grobmyer, E. Scott and B. Moudgil, *Small*, 2012, **8**, 2856.
30 Y. Liu, K. Ai, J. Liu, Q. Yuan, Y. He and L. Lu, *Angew. Chem., Int. Ed.*, 2012, **51**, 1437.
31 Z. Liu, Z. Li, J. Liu, S. Gu, Q. Yuan, J. Ren and X. Qu, *Biomaterials*, 2012, **33**, 6748.
32 X. Zhu, J. Zhou, M. Chen, M. Shi, W. Feng and F. Li, *Biomaterials*, 2012, **33**, 4618.
33 D. Pan, C. Schirra, A. Senpan, A. Schmieder, A. Stacy, E. Roessl, A. Thran, S. Wichline, R. Proska and G. Lanza, *ACS Nano*, 2012, **6**, 3364.
34 Z. Liu, F. Pu, S. Huang, Q. Yuan, J. Ren and X. Qu, *Biomaterials*, 2013, **34**, 1712.
35 E. Matijevic and W. Hsu, *J.Colloid Interface Sci.*, 1987, **118**, 506.
36 N. Lewinski and V. Colvin, *Small*, 2008, **4**, 26.
37 Y. Lin and C. Haynes, *J. Am. Chem. Soc.*, 2010, **132**, 4834.
38 I. Slowing, C. Wu, J. Vivero-Escoto and V. Lin, *Small*, 2009, **5**, 57.
39 H. Zhang, Z. Ji, T. Xia, H. Meng, C. Low-Kam, R. Liu, S. Pokhrel, S. Lin, X. Wang, Y. Liao, M. Wang, L. Li, R. Rallo, R. Damoiseaux, D. Telesca, L. Mädler, Y. Cohen, J. Zink and A. Nel, *ACS Nano*, 2012, **6**, 4349.
40 L. Xiong, T. Yang, Y. Yang, C. Xu and F. Li, *Biomaterials*, 2010, **31**, 7078.
41 M. Li, K. Al-Jamal, K. Kostarelos and J. Reineke, *ACS Nano*, 2010, **4**, 6303.
42 L. Cheng, K. Yang, M. Shao, X. Lu and Z. Liu, *Nanomedicine*, 2011, **6**, 1327.